Macroscopic plasma behavior in a highvoltage toroidal theta pinch

D. P. Murphy, G. C. Goldenbaum, C. ChinFatt, Y. P. Chong, A. W. DeSilva et al.

Citation: Phys. Fluids **26**, 1061 (1983); doi: 10.1063/1.864218
View online: http://dx.doi.org/10.1063/1.864218
View Table of Contents: http://pof.aip.org/resource/1/PFLDAS/v26/i4
Published by the American Institute of Physics.

Macroscopic plasma behavior in a high-voltage toroidal theta pinch

D. P. Murphy,[a] G. C. Goldenbaum, C. Chin-Fatt, Y. P. Chong, A. W. DeSilva, H. R. Griem, R. A. Hess, and R. L. Merlino[b]
Laboratory of Plasma and Fusion Energy Studies, University of Maryland, College Park, Maryland 20742

(Received 6 April 1982; accepted 21 December 1982)

The behavior of the implosion and post-implosion phases of two different toroidal high-beta plasma configurations has been investigated. The plasma is produced in a nominally axisymmetric toroidal theta pinch in which a tokamak-like low-beta plasma is heated and compressed to high beta by a fast-rising toroidal field. The two plasma cases differed from each other by the direction of their initial toroidal magnetic field relative to the direction of the main implosion magnetic field. The purpose of this investigation was to determine what factors govern the development and lifetime of the magnetic configuration during the early time post-implosion phase. It was determined from the q profiles for the parallel field case that the plasma should be unstable to the $m = 1$ kink mode, i.e., $q < 1$, but the normal outward shift of the plasma with respect to the external conducting wall carried it into the internal vacuum chamber wall before the kink could grow to an observable level. The magnetic fields in the case with the initial toroidal field antiparallel to the main implosion magnetic field exhibited nonaxisymmetric behavior.

I. INTRODUCTION

For many years linear theta pinches utilizing implosion heating have been used to produce high-temperature plasmas.[1] In low-density experiments[2] where turbulent effects appear to dominate the heating process, it was found that antiparallel main axial and bias fields produce more energetic plasmas than parallel fields. There are two obvious differences between the two types of configuration. In the antiparallel-field situation there is a null in the axial B_z field and the field lines close around the plasma, i.e., there exists a closed surface reversed-field configuration. Neither of these properties exist in the parallel-field case. In a toroidal theta pinch, however, it is possible to retain the closed property, because field lines remain in the torus without intersecting a wall, with and without the axial field reversal.

The University of Maryland toroidal theta pinch, THOR, was designed and built to study implosion heating without the very rapid thermal and particle end losses inherent in open-ended linear devices. This implosion phase lasts about 1.5 μsec in THOR and has been extensively studied.[3] Since the plasma cannot be ejected out the ends there possibly exists a post-implosion phase in which to study the plasma. The primary diagnostics for this study are magnetic probes and He–Ne laser interferometry. Electron and ion heating measurements during the implosion phase have been reported previously.[4] Similar results have also been obtained in other high-input power-pulsed toroidal pinches.[5,6]

The purpose of this work was to investigate the evolution of the magnetic configuration and plasma density during the post-implosion phase of the experiment after a quasiequilibrium has been obtained. Our experimental approach was first to determine all three orthogonal components of the magnetic field as a function of space and time in a minor cross section of the torus. From these measurements we obtain not only the magnetic fields but also, with certain assumptions, the plasma currents, poloidal and toroidal magnetic fluxes, electric fields, resistivity, plasma kinetic pressure, safety factor (q), and the plasma β. Second, we used interferometry to make a direct measurement of the electron density in the same cross section.

II. EXPERIMENTAL TECHNIQUE

The design parameters of the THOR experiment have been reported before[6] and will not be repeated here except to say that the vacuum chamber has a major radius of 50 cm and a minor radius of 20 cm. The initial plasma has a peak density of $5\times10^{14}\text{cm}^{-3}$ centered at about $r = 55$ cm, an electron temperature of about 10 eV, a B_ϕ field of $\pm$ 800 G, and a toroidal current of about 20 kA. A fast-rising toroidal field ($\tau_{1/4}\simeq1.0$ μsec, $L/R\simeq20$ μsec) with a maximum amplitude of 5–6 kG at the major radius is applied either parallel or antiparallel to the initial bias field.

The magnetic fields during the implosion and post-implosion phases were measured using four sets of three orthogonally oriented inductive loops which measured B_R, B_Z, and B_ϕ. The magnetic data was first separated according to the field component measured and then by (R, Z) position in the cross section [see Fig. 1(a)]. Duplicate shots at each position were averaged and scaled to convert from voltage to magnetic field units. The measured B_R and B_Z field components, here collectively called $\mathbf{B}_{RZ}$, have superimposed upon their values some signal that is proportional to the toroidal magnetic field value, as determined from vacuum shots. This is removed by computer processing using the local toroidal field to reveal the true B_R and B_Z field values.

For each time sample, each field component can now be plotted on a rectangular grid of its (R, Z) positions. The spacing between sampled points is either 1 or 2 cm. The grid mesh was set at 1 cm $\times$ 1 cm because the coils' physical dimensions were on the order of 1 cm. In order to estimate the

[a] Present address: Jaycor, Alexandria, Virginia 22303.
[b] Present address: Department of Physics and Astronomy, University of Iowa, Iowa City, Iowa 55242.

 0031-9171/83/041061-10$01.90

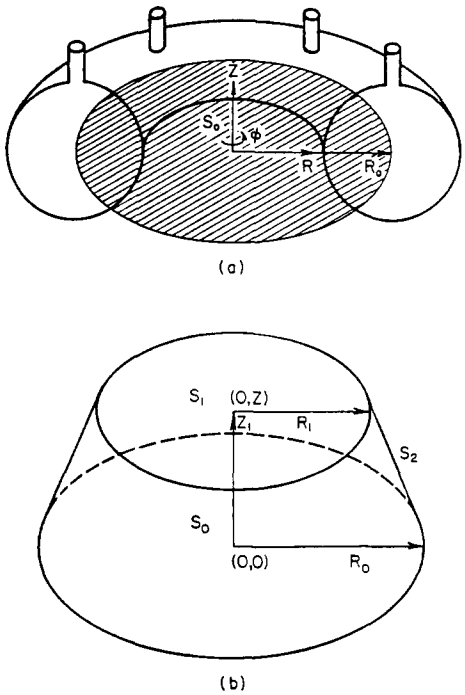

FIG. 1. Surfaces in the region of the torus: (a) flat, circular surface in the midplane of the torus; and (b) surfaces S_0, S_1, and S_2 which form a closed surface.

values of the field component at unsampled grid points, polynomial fitting was utilized. Sampled and unsampled positions were assigned values based on the polynomials. This smoothed the data and averaged out small differences in the probe calibrations.

The magnetic fields can be immediately plotted and can be used to derive various other quantities. Some of these calculations have as an assumption toroidal axisymmetry of all field components, i.e., $\partial/\partial\phi = 0$. Since it was only possible to take data at one value of the toroidal angle, there is no direct evidence to support this assumption. Some indirect evidence can be obtained on the axisymmetry of the toroidal field component from one of Maxwell's equations,

$$\nabla\cdot\mathbf{B} = 0. \tag{1}$$

If B_ϕ is toroidally axisymmetric that would imply,

$$\nabla\cdot\mathbf{B}_{RZ} = 0 = \frac{1}{R}\frac{\partial}{\partial R}(RB_R) + \frac{\partial B_Z}{\partial Z}. \tag{2}$$

If therefore $|\nabla\cdot\mathbf{B}_{RZ}| \leqslant \epsilon$, where ϵ is comparable to the uncertainty in the data, this would be deemed strong experimental evidence for the validity of the toroidal axisymmetry assumption.

The RZ current density, $\mathbf{J}_{RZ}$, is calculated quantity partially dependent on toroidal axisymmetry,

$$\mathbf{J}_{RZ} = \frac{c}{4\pi}\left[\left(\frac{1}{R}\frac{\partial B_Z}{\partial\phi} - \frac{\partial B_\phi}{\partial Z}\right)\hat{R} + \left(\frac{1}{R}\frac{\partial(RB_\phi)}{\partial R} - \frac{1}{R}\frac{\partial B_R}{\partial\phi}\right)\hat{Z}\right]. \tag{3}$$

Derivatives of B_R and B_Z with respect to ϕ are neglected in the calculation. However, since B_R and B_Z are at least an order of magnitude smaller than B_ϕ and since our pinch characteristically has large gradients in the toroidal field, a small lack of toroidal axisymmetry should not significantly alter the result of the calculation.

Let ψ define the poloidal flux,

$$\psi = \int \mathbf{B}_{\rm pol}\cdot d\,\mathbf{S}_{\rm pol}, \tag{4}$$

which is a quantity more intimately tied to the assumption of toroidal axisymmetry [see Fig. 1(a)]. Let S_0 be the flat circular surface centered in the $Z = 0$ plane of the torus with radius R_0. ψ_0 is the (unknown) flux through this surface. One can see from the figure that part of S_0 is outside the vacuum vessel, so ψ_0 cannot be computed directly since we have no measurement there due to the way the coils are constructed. Let S_1 be the flat surface with radius R_1, concentric with S_0, a distance Z_1 above S_0. S_1 is also partially outside the vacuum vessel [see Fig. 1(b)]. ψ_1 is the (also unknown) flux through S_1. Let S_2 be the surface bounded by S_0 and S_1 which makes a closed surface with S_0 and S_1. The closed surface looks like a truncated cone. S_2 is a surface wholly inside the accessible region of the vacuum vessel.

Gauss's law assures that

$$\int \mathbf{B}_{\rm pol}\cdot d\,\mathbf{S}_0 + \int \mathbf{B}_{\rm pol}\cdot d\,\mathbf{S}_1 + \int \mathbf{B}_{\rm pol}\cdot d\,\mathbf{S}_2 = \psi_0 + \psi_1 + \psi_2 = 0, \tag{5}$$

so

$$\psi_1 = -\psi_2 - \psi_0. \tag{6}$$

Thus at each point (R_1, Z_1) inside the torus the flux ψ_1 is determined by the unknown ψ_0 and the calculated ψ_2. ψ_0 will change by some unknown amount from time step to time step. Nevertheless, plots of contours of constant poloidal flux made at different times will show how the flux surfaces evolve in time.

To calculate ψ_2 again we assume toroidal axisymmetry to simplify the calculation

$$\int_{R_0Z_0}^{R_1Z_1} \mathbf{B}_{\rm pol}\cdot d\hat{S}_2 = \int_0^{2\pi}\int_{R_0}^{R_1}\int_{Z_0}^{Z_1} (B_R\hat{R} + B_Z\hat{Z})\cdot(R\,d\phi\,dl\,\hat{S}). \tag{7}$$

The increment dl is along a contour from (R_0, Z_0) to (R_1, Z_1). This path need not be a straight line and can be arbitrary path. We can simplify the integration if we pick a path that is a series of horizontal and vertical steps (see Fig. 2). The sur-

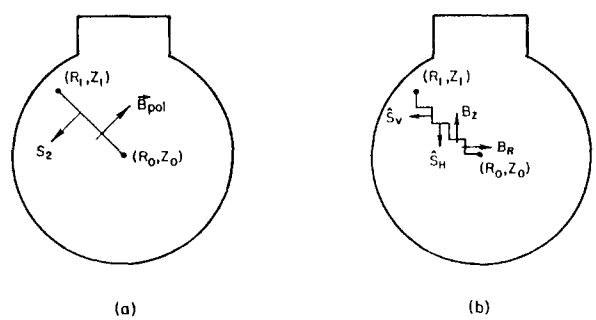

FIG. 2. Surfaces used in calculating the poloidal flux: (a) poloidal magnetic field intersecting surface S_2; and (b) actual surfaces and magnetic field components used in calculating the poloidal flux.

face integral breaks up into a sum of short line integrals over the horizontal and vertical segments. We get ψ_2 as

$$\psi_2 = 2\pi\left(\sum_{V_i} R_i \int_i B_R\, dZ + \sum_{H_j} \int_j B_Z R\, dr\right). \tag{8}$$

The magnetic field is everywhere tangent to a flux surface. A flux surface has a constant poloidal flux value ψ at every point on its surface. This flux surface also encloses a toroidal flux value

$$\chi = \int \mathbf{B}_\phi \cdot d\,\mathbf{S}_\phi. \tag{9}$$

Having measurements of both fluxes we can calculate the safety factor q which is defined as

$$q = \frac{d\chi}{d\psi}. \tag{10}$$

Equilibrium requires the complete balance of forces in a closed system. In the magnetohydrodynamic (MHD) model of equilibrium with scalar plasma pressure, the pressure gradient is balanced by magnetic forces allowing us to calculate the pressure gradient from the field measurements,

$$\nabla P = (1/4\pi)(\nabla\cdot\mathbf{B})\cdot\mathbf{B}. \tag{11}$$

We realize that the THOR plasma is very short-lived, which perhaps makes assumptions inherent to equilibrium MHD theory somewhat dubious.

Finally, we can determine upper and lower bounds on two important plasma parameters, $\beta_{\rm pol}$ and β,

$$\beta_{\rm pol} = 8\pi\langle P\rangle/\langle B_{\rm pol}^2\rangle, \tag{12}$$

$$\beta = 8\pi\langle P\rangle/\langle B^2\rangle, \tag{13}$$

$$\langle X\rangle = \frac{\int X\, d^3x}{\int d^3x}. \tag{14}$$

There are three interesting regimes for $\beta_{\rm pol}$,[7]

$\beta_{\rm pol} = 1$, $\quad \nabla P \cong (1/c)(\mathbf{J}_\phi \times \mathbf{B}_{\rm pol})$,

$\beta_{\rm pol} \ll 1$, $\quad \nabla \mathbf{P} = 0$,

$\beta_{\rm pol} \gg 1$, $\quad \nabla P \cong (1/c)(\mathbf{J}_{\rm pol} \times \mathbf{B}_\phi)$.

We will see that both the parallel and antiparallel bias cases showed $\beta_{\rm pol} \gg 1$. The average β from Eq. (13) can only be assigned upper and lower limits since the field of view does not include the entire cross section of the torus.

III. RESULTS AND INTERPRETATIONS OF MAGNETIC AND INTERFEROMETRIC DATA

A. Introduction

Some of our magnetic and interferometric data are presented at the end of this section to Figs. 3–6 for both the cases of bias field parallel (↑↑) and antiparallel (↑↓) to the fast-rising main toroidal magnetic field. Both bias cases are presented side by side for each property of the discharge.

B. Initial conditions

Ideally the initial conditions of the plasma for the two cases would be identical save for the direction of the initial toroidal field. The crowbarred bias field and the ringing preheater field are both toroidal fields and they combined to produce the net initial toroidal field. The bias field was reversed but the preheater field was not reversed. The ringing preheater field causes the gas in the torus to ionize and compress slightly during alternate half-cycles when the preheater and bias fields are opposite. Because of this the main toroidal field pulsers are triggered about ½ preheater cycle ($\simeq$10 μsec) earlier in the ↑↑ case than in the ↑↓ case. The toroidal current distribution seems to depend heavily on the initial plasma conditions. In the ↑↓ case the data show that the plasma is situated about 5 cm below the $Z = 0$ plane and the toroidal current runs predominately about 10 cm below the $Z = 0$ plane at $T = 0.0$ μsec relative to the start of the compression field. Both the toroidal current and the plasma are nearly in the $Z = 0$ plane in the ↑↑ case.

C. Toroidal field

The toroidal field provides a good indication of the plasma distribution since, at least initially, the poloidal current is the dominant component of the total current. The data for the ↑↑ case show a rapid diffusion of the toroidal field into the plasma. By $T = 0.8$ μsec after the start of the main compression field, the field at the center of the plasma rises to 80% of the value it would have if the field were a vacuum $1/R$ distribution. For a short time near LC crowbar time ($T = 1.2$ μsec) the ↑↑ case becomes slightly paramagnetic, i.e., the toroidal field inside the plasma is larger than the vacuum field would be. The plasma then regains a mild diamagnetic profile and maintains it until the plasma hits the wall near $T = 3$ μsec.

The toroidal field in the ↑↓ case exhibits considerably different behavior. The field does not immediately penetrate to the plasma core but instead traps the bias toroidal field and compresses it until the magnitude of the field at the center of the plasma increases from its initial value of -500 G to -2000 G. Consequently, the diamagnetic well is about 4000 G deep. This negative toroidal field is gradually annihilated as the compression field penetrates into the plasma. However, some negative field still remains after the plasma hits the outer wall. A dotted contour on the ↑↓ $RB_{\rm tor}$ plots mark the boundary between the positive compression field and the negative bias field. The outward drift of the plasma column carries it into the outer wall near $T = 4$ μsec (see Fig. 3).

D. $\mathbf{B}_{RZ}$ field and its derivative quantities

In this paper we have used the term RZ to mean the $\hat{R}$ and $\hat{Z}$ components of a vector quantity, such as using $\mathbf{B}_{RZ}$ to collectively identify the B_R and the B_Z fields in a (R, ϕ, Z) coordinate system. The measured $\mathbf{B}_{RZ}$ field can be produced by toroidal plasma currents and by toroidal currents outside the vacuum vessel. Near the inner edge of the vacuum vessel we find up to a 400 G field oriented predominately in the $\hat{Z}$ direction (see Fig. 4). This field is generated by the toroidal current running along the copper gasket in the inner edge of the main toroidal field coil. The field penetrates the vacuum vessel through the coil slot. The current running along the copper gasket is started well before the main implosion current is started. If one examines the $\mathbf{B}_{RZ}$-field plots for times

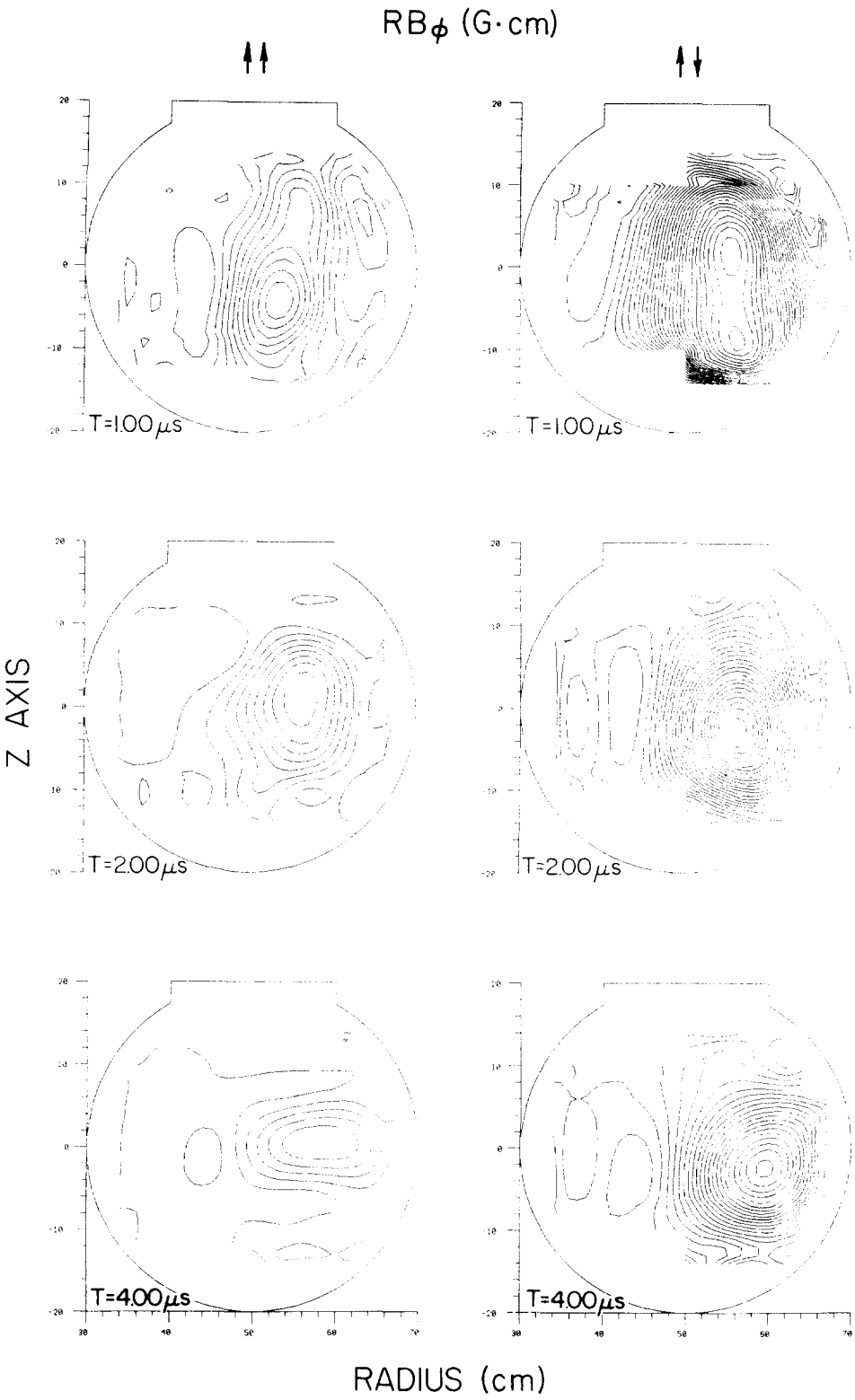

FIG. 3. Contour maps of RB_ϕ for the parallel and antiparallel bias cases at three different times during the main compression.

well before the implosion is triggered, one finds that near the inner edge of the torus the $\mathbf{B}_{RZ}$ field mirrors the time history of the current in the gasket.

Near the outer edge of the vacuum vessel we usually see a large radial magnetic field. It is seen even during vacuum shots with only the main implosion field. Its origin is a slight bulge of the implosion field near the slot between the coil sections. The field loses its toroidal axisymmetry near the slot. Since the implosion field is several kG, a slight deviation from the $\hat{\phi}$ direction readily produces a measurable $\hat{R}$ field. Whenever the implosion field deviates from toroidal axisymmetry, it can produce $\hat{R}$- and $\hat{Z}$-field components.

The third source is the $\mathbf{B}_{RZ}$ field generated by the toroidal current running in the plasma itself. Based on the net toroidal current measured by a Rogowski loop around the minor circumference of the torus, this field should be at most

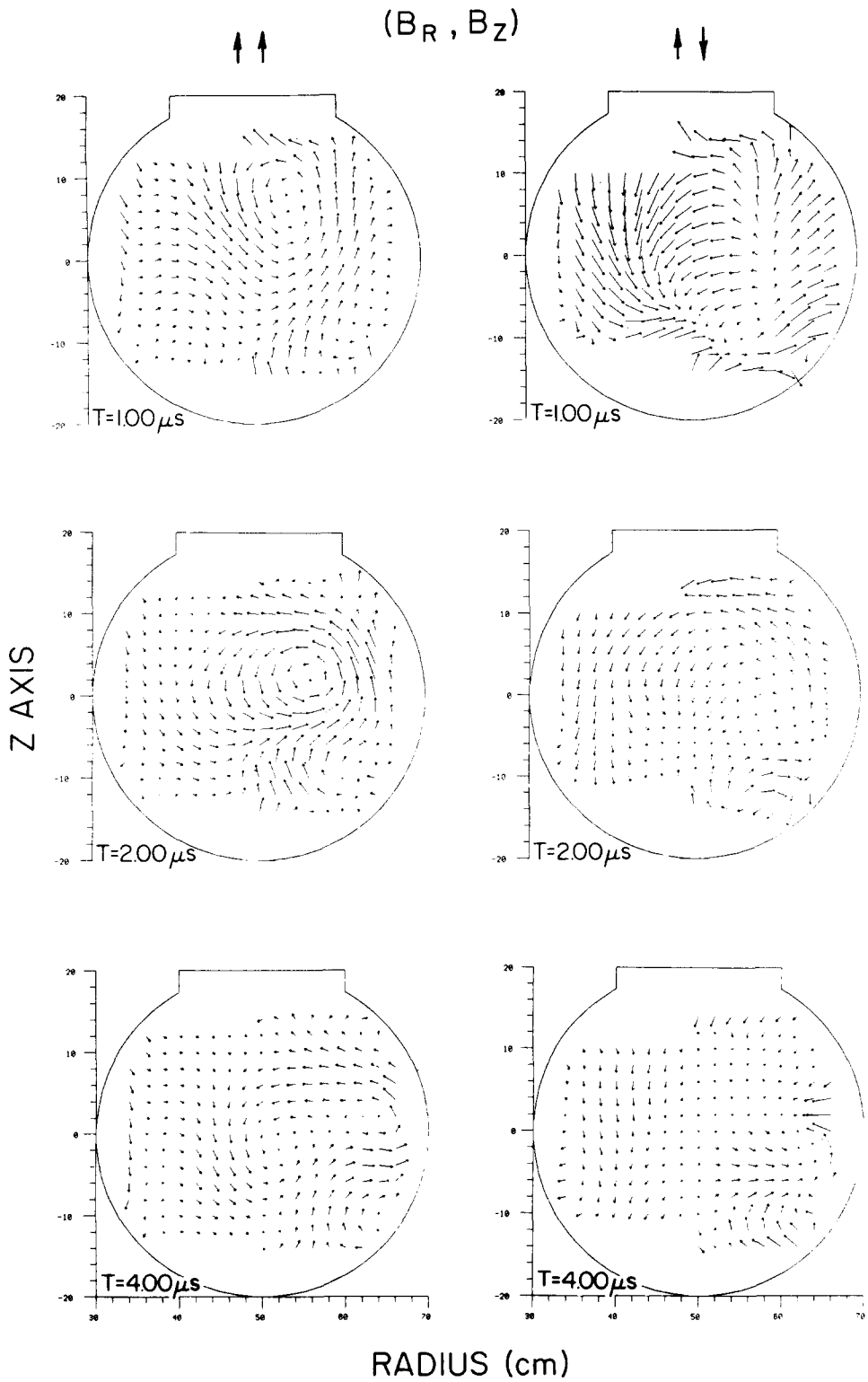

FIG. 4. Vector maps of (B_R, B_z) for the parallel and antiparallel bias cases at three different times during the main compression.

400 G. It is evident from the $\mathbf{B}_{RZ}$ plots that substantially more than 400 G was sometimes measure.

The large current driven by the main implosion field can locally deviate from toroidal axisymmetry due to plasma effects and/or due to the large slots between the coil sectors. Thus the main implosion current can have a localized component in the toroidal direction. At best, we can examine the $\mathbf{J}_\phi$ profiles and judge that some part of the profile might be due to true axisymmetric toroidal current and some other part is due to the lack of toroidal axisymmetry of the main implosion current. To quantify this judgment $\nabla\cdot\mathbf{B}_{RZ}$ was calculated [Eq. (2)]. One cannot expect $\nabla\cdot\mathbf{B}$ to be exactly zero due to uncertainties in the measurements of the field components and due to the polynomial interpolation that smoothed the data. At best, $|\nabla\cdot\mathbf{B}| = \epsilon$, where ϵ is a relatively small number of approximately 25 G/cm.

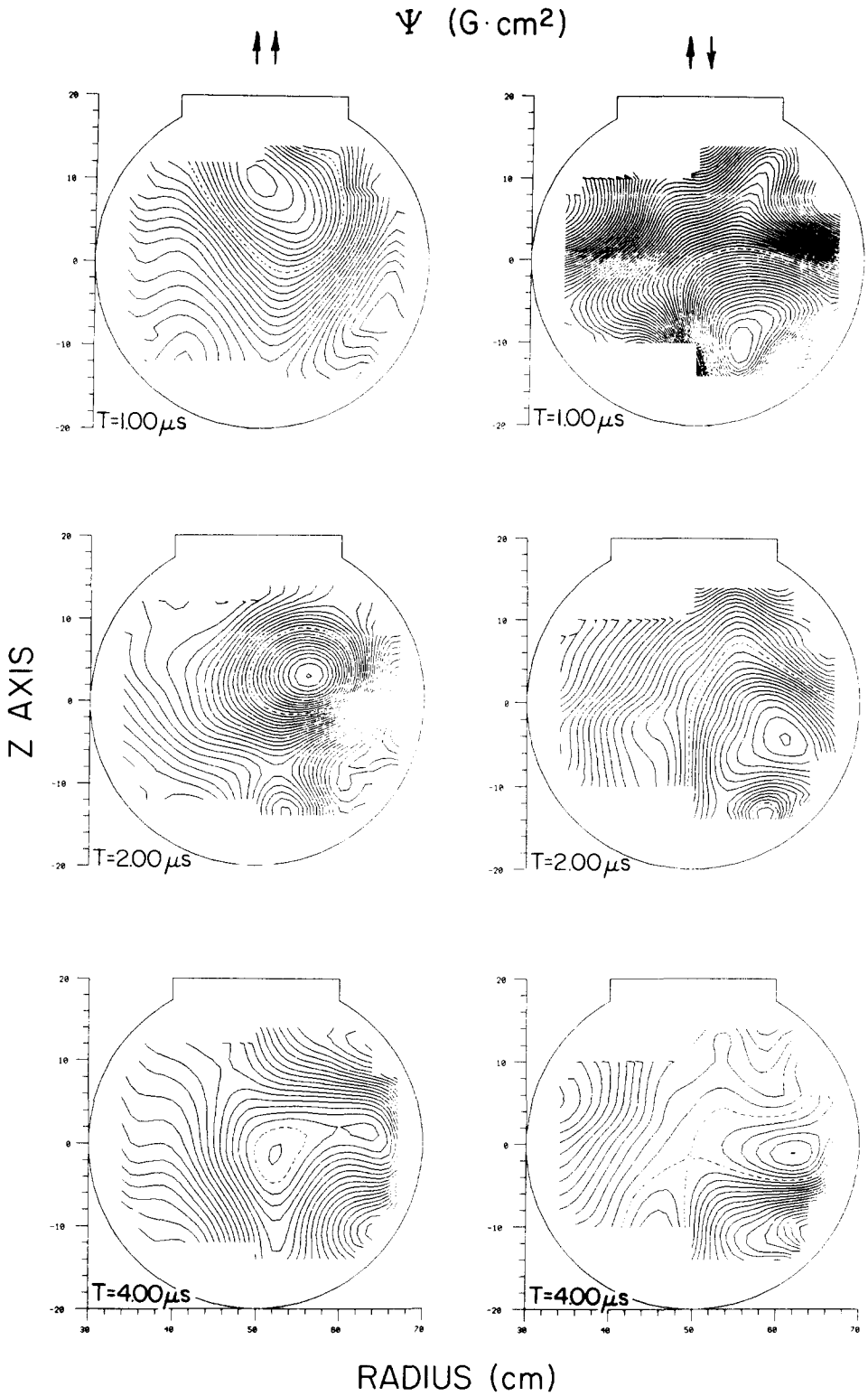

FIG. 5. Contour maps of poloidal flux Ψ for the parallel and antiparallel bias cases at three different times during the main compression.

Except during the implosion the ↑↑ case showed $\nabla \cdot \mathbf{B}_{RZ}$ to be small, indicating a high degree of toroidal symmetry. Also, from $\nabla \times \mathbf{B}_{RZ}$ we found that the $\mathbf{B}_{RZ}$ field is predominantly a product of the toroidal plasma current. The ↑↓ case showed $|\nabla \cdot \mathbf{B}_{RZ}|$ equal to several times ϵ throughout the plasma lifetime and to be rather large during the implosion. Therefore, the $\mathbf{B}_{RZ}$ field in the ↑↓ case is partially due to a lack of axisymmetry.

E. Poloidal flux

As described in Sec. III, the poloidal flux is calculated from the measure B_R and B_Z fields along a path of vertical and horizontal steps from ($R_0 = 50$, $Z_0 = 0$) to (R_1, Z_1) assuming axisymmetry. The flux at (R_0, Z_0) was arbitrarily set to zero and the contour through (R_0, Z_0) drawn as a dotted line.

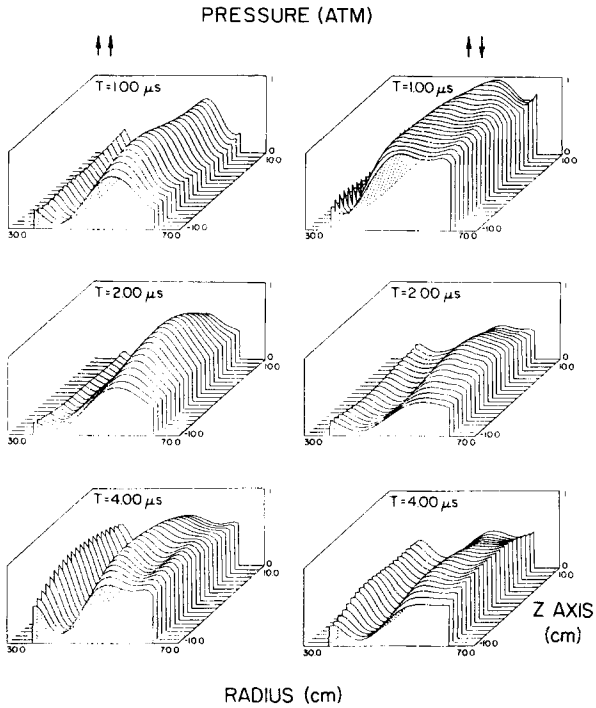

FIG. 6. Contour maps of pressure for the parallel and antiparallel bias cases at three different times during the main compression.

In ideal MHD with toroidal axisymmetry, $I = RB_\phi$ and poloidal flux ψ are constant on a flux surface while B_ϕ and B_{RZ} are tangent to the surface. The comparison of all these quantities in Figs. 3–5 for the ↑↑ case shows surprising compatibility considering the short lifetime of the experiment. Late in time the poloidal flux contours begin to elongate and disrupt. However the entire experiment is over in about 2–4 Alfvén transit times for the ↑↑ case and about 5–6 transit times in the ↑↓ case. The disruption of the flux contours is therefore more likely due to the plasma hitting the wall than due to MHD instability.

The flux surfaces calculated for the ↑↓ case bear little or no resemblance to the RB_ϕ contours. Also the $\mathbf{B}_{RZ}$ field vectors should be tangent to the calculated flux surfaces, but are not. This may be in part due to external contributions to the $\mathbf{B}_{RZ}$ fields and in part due to a lack of toroidal axisymmetry of the main implosion field. Externally produced $\mathbf{B}_{RZ}$ fields apparently contribute significantly to the poloidal flux calculation in this case (see Fig. 5).

F. Pressure and line density

The pressure profiles are presented as three-dimensional plots. The plot limits are 30 cm$\leqslant R \leqslant$70 cm and -10 cm$\leqslant Z \leqslant$10 cm, while the output data limits are 36 cm$\leqslant R \leqslant$64 cm; -10 cm$\leqslant Z \leqslant$10 cm. The plot regions $R < 36$ cm and $R > 64$ cm are set to zero. The sharp transitions from the data region to the boundary region are not to be construed as large pressure gradients. They are merely visual aids to help keep track of the position and the amplitude of the curves.

If the plasma were in MHD equilibrium, then the magnetic pressure gradients would balance the particle pressure gradients. The particle pressure profiles presented here assume equilibrium exists and are derived directly from Eq. (11). The integrations of $\partial P/\partial R$ and $\partial P/\partial Z$ contained an unknown integration constant that changed from time step to time step. Since pressure is a positive quantity, the calculated values at each time step were adjusted so the most negative value was adjusted upward to zero. However, if no point in the field of view truly had zero pressure than the pressure contour plots show only how the pressure varies within the field of view. Since the field of view extends inside to $R = 36$ cm and most of the plasma is at $R > 50$ cm and drifting outward, the constant is probably not too different from zero.

If we take the line density plots determined by interferometry at constant major radius and use the RB_ϕ plots to get a measure of the height of the plasma along the line density path, we can estimate the average plasma density. We use the RB_ϕ contours because they follow the calculated pressure profiles very closely. In the ↑↑ case the maximum line density of about $3\times10^{16}/\text{cm}^2$ occurs at $T = 1.0$ μsec and $R = 55$ cm. The plasma is elongated slightly and is about 25 cm high. This determines an average electron density $\bar{n}_e$ of $1.2\times10^{15}/\text{cm}^3$. The maximum of the line density reaches the same value of $3\times10^{16}/\text{cm}^2$ at $T = 1.5$ μsec and $R = 55$ cm for the ↑↓ case. The plasma shape here is more circular and only 20 cm across. This gives $\bar{n}_e = 1.5\times10^{15}/\text{cm}^3$.

Estimates of the electron and ion temperatures were made from x-ray studies and from impurity ion (carbon) spectral line broadening, respectively.[6] The deuterium ion temperatures quoted below are not inconsistent with the measured impurity ion temperatures. It is reasonable to assume quasineutrality on the average through the plasma, so $n_e = n_i = n$. The total pressure is then: $P = nk(T_e + T_i)$. If we compare the pressures calculated from the density and temperature and the pressures calculated from the magnetic fields P_m we get the results shown in Table I. The pressures calculated by two different methods agree to well within estimated errors.

One might question the validity of using MHD equations to calculate the pressure. A more detailed hybrid-kinetic model of the plasma, using fluid electrons and Vlasov ions, developed for use in pinch experiments yielded the same results as the simpler MHD theory, subject to minor restrictions; namely, that timescales be long compared to the electron cyclotron time and that scale lengths be long compared to the electron gyroradius.[8] Both these restrictions are fulfilled by the THOR plasma experiment.

G. Safety factor and plasma beta

In some theoretical models the HBT has a critical β value β_c above which the plasma is unstable for any value of q on the magnetic axis. Marder[9] found for a sharp boundary model of a HBT that large β could be reached for a nearly circular plasma with $q_{\text{axis}} \gtrsim 1$. Freidberg and Haas[10] and Freidberg and Grossman[11] extended this analysis to toroidal plasmas. In THOR, for a circular plasma with $q_{\text{axis}} < 2$, the maximum stable β would be about 6%. The plasma would be unstable for any β if $q_{\text{axis}} < 1$ because of the $m = 1$ kink mode. More recent work by An and Bateman[12] in a rectan-

TABLE I. Comparisons of pressure.

Case	Time	No./cm^3	T_e	T_i	$nk(T_e + T_i)$	P_m
↑↑	1.0	1.2×10^{15}	$\leqslant$100 eV	$\simeq$400 eV	6×10^5	8×10^5 erg/cm^3
↑↓	1.5	1.5×10^{15}	250 eV	$\simeq$350 eV	9×10^5	8×10^5 erg/cm^3

gular cross section tokamak found that the optimum plasma shape for maximizing β is a mildly vertically elongated cross section with rounded ends. They calculated a maximum stable β of 3% for a diamagnetic plasma with this optimum shape.

The safety factor, $q = \Delta\chi/\Delta\psi$, was calculated from the measured magnetic fields for the closed poloidal flux surfaces in the ↑↑ bias case at several different times. The ↑↓ bias q could not be calculated directly from the measured fields because of the previously mentioned difficulties with the poloidal-flux calculation. In Fig. 7 we show some of the calculated q profiles at different times for the ↑↑ case. In Fig. 8 we show the single q profile we have for the ↑↓ case. In Figs. 7 and 8 note that $q_{\text{axis}} < 1$ for time $< 3.0\,\mu$sec, and that $q_{\text{axis}} < 2$ for all time. The one ↑↓ case profile has $q < 1$ also.

Measurements of beta were attempted but due to the limited field of view an accurate value was difficult to obtain. Minimum values of the volume averaged beta ranged from 3%–5% for the parallel case and approximately 10% for the antiparallel case.

H. Resistivity and Ohmic heating

We have determined the current density from the magnetic field measurements. We can estimate the resistivity from Ohm's law,

$$E_\theta - (\boldsymbol{\eta}\cdot\mathbf{J})_\theta + V_{er}B_\phi/c = 0. \tag{15}$$

This can be further simplified if we evaluate the equation either at the instant of maximum magnetic compression (i.e., when the radial velocity goes to zero) or at a field zero,

$$\eta_\perp = E_\theta/J_\theta \simeq E_{RZ}/J_{RZ}. \tag{16}$$

So once we have E_{RZ} we can find the resistivity. Since B_ϕ only goes to zero in the reverse-field case for consistency we chose to evaluate the equation on the surface of maximum current density at times for which the magnetic structure is stationary, which should closely correspond to zero radial flow velocity.

We can estimate $\mathbf{E}_{RZ}$ in much the same way one calculates magnetic fields from known current profiles. Maxwell's equations for **E** and **B** have similar form. If mathematically we substitute for a filament of current **J** a "filament" of $\partial\mathbf{B}/\partial t$ at each grid point we can calculate **E** using the analog of the Biot–Savart law. Our calculation only includes those grid points within the field of view and so is only an estimate for **E**.

Using $|E_{RZ}|$ estimated in this manner we obtain the estimates for η shown in Table II. The values of η_θ are at best accurate to $\pm$ 50% but are still well within the bounds of previous experimental estimates of the resistivity for a theta pinch. Note, the classical Spitzer resistivity for these temperatures ($T_e \approx 200$ eV) is $\eta_\perp \simeq 6\times10^{-17}$sec, about three orders of magnitude smaller than our experimental values.

The resistivity of the ↑↑ case is larger than the resistivity of the ↑↓ case. The higher the resistivity, the faster magnetic

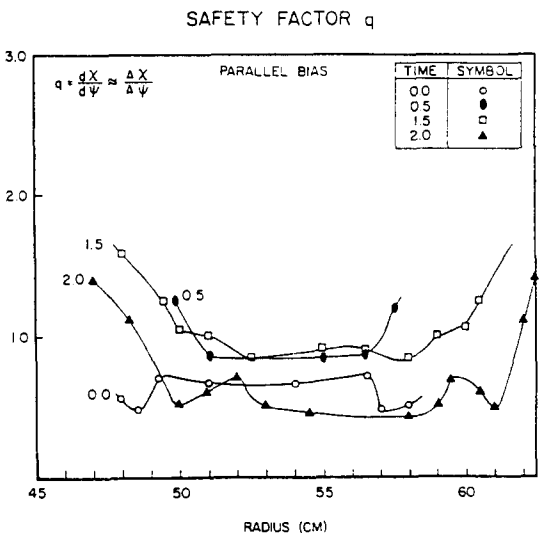

FIG. 7. Profiles across the radius of the torus of the safety factor for the parallel bias case at different times during the main compression.

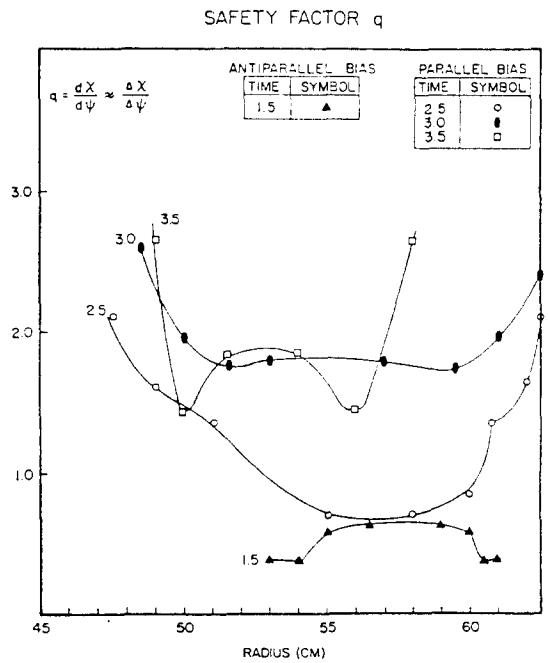

FIG. 8. Profiles across the radius of the torus of the safety factor for the antiparallel and parallel bias cases at different times during the compression.

TABLE II. Estimates for η.

Case	Time(μsec)	E_{RZ}(SV/cm)	J_{RZ}(SA/cm^2)	η_θ(sec)	$\eta_\theta J_{RZ}^2$(erg/cm^3/sec)
↑↑	0.8	0.5	1×10^{12}	5×10^{-13}	5×10^{11}
↑↓	1.4	0.2	1.7×10^{12}	1.2×10^{-13}	3.5×10^{11}

field will penetrate into a plasma, so this result was expected. Even though the antiparallel case resistivity is lower, its narrow current sheath and its large current density combine to keep the sheath region hotter than the bulk of the plasma well after the peak of the implosion.

IV. SUMMARY AND CONCLUSIONS

We have produced two high-β plasma conditions in the THOR experiment that are primarily distinguished by different directions of their initial toroidal field. The ↑↓ case is characterized by a narrow poloidal (RZ) current sheath which is centered about the null toroidal field surface and which implodes to its minimum diameter in 1.5 μsec. The peak current density is 0.7 kA/cm^2 and the resistivity, which was measured well away from the null contour, is $\eta_\perp \approx 1.2\times10^{-13}$sec. There is evidence that high-energy electrons are generated in this sheath and that they diffuse rapidly into the bulk of the plasma. The bulk electron temperature peaks at 250 eV at $T = 1.5$ μsec.[6] The ↑↑ case is characterized by a more diffuse RZ current sheath which implodes to its minimum diameter in 0.75 μsec. The peak current density is at most 0.3 kA/cm^2 and the resistivity is $\eta_\perp \approx 5\times10^{-13}$sec. This higher value of the resistivity is consistent with the rapid penetration of the main implosion field into the plasma. Both resistivity values exceed the Spitzer resistivity by three orders of magnitude. There was evidence of a small percentage ($\leqslant 1\%$) of high-energy electrons, but the bulk electron temperature was probably less than 75 eV.

The toroidal current distribution is governed by the heating in the poloidal current sheath. At early times the toroidal current flows in the hotter sheath region outside the bulk of the plasma. When the bulk of the plasma and the sheath reach a common temperature, the toroidal current is seen to reenter the central region. A toroidal current of about 20 kA was driven in both plasma cases by the combined effects of the transformer and the toroidal driver (TD) banks.[6] The 20 kA toroidal current is already too much at the small toroidal field for stability. The safety factor q is at times significantly less than one inside the plasma for both cases. This makes the plasma vulnerable to the fast growing MHD instability, the $m = 1$ kink mode. As the experiment is now configured, the plasma drifts to the outer dielectric wall before the kink mode could grow to an observable level. It can be shown that q is proportional to the RZ current and inversely proportional to the toroidal current. The safety factor can be raised by increasing the RZ current and/or lowering the toroidal current. If the THOR machine were stressed to its maximum rated capacity, I_{RZ} could be increased by at most a factor of two. Even then I_ϕ would probably have to be reduced to get q above 1.0 in the plasma core.

The plots of $\mathbf{B}_{RZ}$, $\mathbf{J}_{\text{tor}}$, and poloidal flux point to a great deal of nonaxisymmetric behavior of the plasma in the ↑↓ case compared to the ↑↑ case. One possible explanation is the reconnection of the magnetic field lines from the initial reversed field to the main implosion field. In the region of the reconnection, the implosion field would have significant R- and Z-field components, such as we have found. Normally the slits between the coil sectors are kept very small ($\simeq$1–2 cm) to reduce field errors. However, installation of a large diagnostic port required modification of the adjoining coil sectors.[6] The gap here is as much as 8 cm. This gap could cause a major perturbation of the magnetic field in the nearby region at the start of the implosion. If a forced reconnection of field lines is taking place, it would occur as the magnitude of the implosion field is increasing and propagate from the gap inward with the implosion. If the reconnection were a result of a tearing mode instability it would take at least one Alfvén transit time across the plasma sheath to grow[13] and would first appear some distance from the gap. Thus the two mechanisms would be distinguishable. One must point out that at present the evidence for reconnection in THOR is only circumstantial because data were taken at only one toroidal angle ϕ_0. To directly verify reconnection and the causal factor one would need field measurements at other angles closely spaced on either side of ϕ_0.

ACKNOWLEDGMENTS

We are grateful to Kenneth R. Diller and David L. Miller for their excellent technical support in the construction and operation of this experiment and to Eugene Day for his expertise with the data acquisition system.

Some of the material in this article is part of a thesis submitted by Donald P. Murphy in partial fulfillment of the requirements for the Doctor of Philosophy degree at the University of Maryland.

This work was supported by the U.S. Department of Energy.

[1] A. C. Kolb, in *Proceedings of the Second United Nations Conference on the Peaceful Uses of Atomic Energy* (United Nations, Geneva, 1958), Vol. 31, p. 328.

[2] W. D. Davis, A. W. DeSilva, W. F. Dove, H. R. Griem, N. A. Krall, and P. C. Liewer, in *Plasma Physics and Controlled Nuclear Fusion Research, Madison, Wisconsin, 1971* (IAEA, Vienna, 1972), Vol. III, p. 289.

[3] Y. G. Chen, C. Chin-Fatt, Y. P. Chong, A. W. DeSilva, G. C. Goldenbaum, H. R. Griem, R. A. Hess, R. L. Merlino, and D. P. Murphy, Phys. Rev. Lett. **38**, 1400 (1977).

[4] R. L. Merlino, G. C. Goldenbaum, C. Chin-Fatt, Y. P. Chong, A. W. DeSilva, H. R. Griem, R. A. Hess, and D. P. Murphy, Phys. Fluids **24**, 2358 (1981).

[5] G. E. Georgiou, T. C. Marshall, and P. G. Weber, Phys. Fluids **23**, 2085 (1980).

[6] F. Soldner, Phys. Fluids **21**, 1036 (1978).

[7]G. Bateman, MHD *Instabilities* (MIT Press, Cambridge, MA, 1978), p. 69.
[8]D. D'Ippolito, Phys. Fluids **18**, 1507 (1975).
[9]B. M. Marder, Phys. Fluids **17**, 440 (1974).
[10]J. P. Freidberg and F. A. Haas, Phys. Fluids **17**, 440 (1974).
[11]J. P. Freidberg and W. Grossman, Phys. Fluids **18**, 1494 (1975).
[12]C. H. An and G. Bateman, Phys. Fluids **22**, 1517 (1979).
[13]J. H. Irby, J. F. Drake, and H. R. Griem, Phys. Rev. Lett. **42**, 228 (1979).